1-1-2004

Single-Phase Flow and Heat Transport and Pumping Considerations in Microchannel Heat Sinks

S V. Garimella
Purdue University, sureshg@purdue.edu

Vishal Singhal

Garimella, S V. and Singhal, Vishal, "Single-Phase Flow and Heat Transport and Pumping Considerations in Microchannel Heat Sinks" (2004). *CTRC Research Publications.* Paper 58.
http://dx.doi.org/10.1080/01457630490248241

Single-Phase Flow and Heat Transport and Pumping Considerations in Microchannel Heat Sinks[†]

Suresh V. Garimella[‡] and Vishal Singhal
NSF Cooling Technologies Research Center
School of Mechanical Engineering, Purdue University
585 Purdue Mall, West Lafayette, IN 47907-2088 USA

ABSTRACT

Microchannel heat sinks are widely regarded as being amongst the most effective heat removal techniques from space-constrained electronic devices. However, the fluid flow and heat transfer in microchannels is not fully understood. The pumping requirements for flow through microchannels are also very high and none of the micropumps in the literature are truly suitable for this application. Results are reported from a wide-ranging research program being conducted on microchannel heat sinks and micropumps to understand fluid flow and heat transfer in microchannels and to identify pumping requirements and suitable mechanisms for pumping in microchannels. In particular, experiments have been performed to show that conventional correlations for fluid flow and heat transfer adequately predict the behavior in microchannels of hydraulic diameters as small as 250 μm. Pumping requirements of microchannel heat sinks have been analyzed, and the size of the microchannels optimized for minimum pumping requirements. Results are also provided from a comprehensive review of micropumping technologies in the literature.

[†] Submitted for publication in *Heat Transfer Engineering*, January 2003, and in revised form March 2003.

[‡] Author to whom correspondence should be addressed; Tel: (765) 494-5621, Fax: (765) 494-0539, sureshg@ecn.purdue.edu

NOMENCLATURE

A	surface area (m^2)
c_p	specific heat (J/Kg K)
d/dx	gradient along length of microchannels (m^{-1})
D	diameter (m)
f	friction factor (dimensionless)
h	heat transfer coefficient (W/m^2 K)
H	height (m)
k	thermal conductivity (W/m K)
L	length (m)
n	number of channels (dimensionless)
Nu	Nusselt number (dimensionless)
q	heat removal rate (W)
Q	volume flow rate (m^3/s)
Re	Reynolds number (dimensionless)
t	thickness (m)
T	temperature (K)
U	mean flow velocity (m/s)
W	width (m)
x^+	entrance length (m)

Greek Symbols

α	aspect ratio, H_c/W_c (dimensionless)
μ	dynamic viscosity (kg/m s)
ρ	density of fluid (kg/m^3)
Δp	pressure drop (Pa)

Subscripts and Superscripts

*	optimal

3 3-sided

4 4-sided

app apparent

c channel

d die

f fluid

fd fully developed

h hydraulic

i inlet

m mean

max maximum

o outlet

s substrate

w wall

x axial coordinate

INTRODUCTION

The use of microchannels for high power-density electronics cooling has been widely studied. Along with providing very high heat transfer coefficients, microchannel heat sinks have the added benefit of being very compact in size, which enhances their suitability to electronics cooling.

Because of the microscale sizes of these channels, great care needs to be exercised in the experimental techniques utilized for their study. In addition, the behavior of microchannels can be different from the corresponding macroscale channels, since the various forces affecting flow and heat transfer scale differently, and take on different levels of predominance as the dimensional scales are reduced.

Various aspects of transport in microchannels relevant to electronics cooling applications are discussed in the present work. The results of studies in the literature on fluid flow and heat transfer through microchannels are first compared and inconsistencies identified. Fluid flow and heat transfer experiments conducted on channels of hydraulic diameter ranging from 250 to 1000 μm are then presented, and results from these experiments compared to predictions from conventional correlations. The pumping requirements of microchannel heat sinks are derived, along with a method to assess the suitability of a given pump to a microchannel heat sink application. Optimization of microchannel dimensions for a specified thermal load, so as to minimize the pumping requirements, is also discussed. Finally, various micropumps presented in the literature are reviewed in terms of their suitability to electronics cooling.

FLUID FLOW AND HEAT TRANSFER

Transport in microchannels has been investigated widely over the last two decades. Quantitative comparisons of the experimental results in the literature show that there are large deviations amongst these studies, not only in magnitudes but also in trends of variation of friction factor and Nusselt number.

Literature Review

A comprehensive review of studies in the literature on fluid flow and heat transfer through microchannels is available in [1]. The emphasis of the review was on experimental results obtained with micro- and mini-channels and tubes. Investigations of boiling and two-phase flows in microchannels, minichannels and small tubes, gas flow in microchannels, analytical studies on microchannel flows, and design and testing of microchannel heat sinks for electronics cooling were

also reviewed. Results for single-phase conditions, quantified in terms of friction factor and Reynolds number for fluid flow and in terms of Nusselt number and Reynolds number for heat transfer, were compared to predictions from conventional correlations both in laminar and turbulent regimes in an earlier paper by Sobhan and Garimella [2].

The product of friction factor and Reynolds number is plotted against Reynolds number in Figure 1 from experimental studies in the literature [3-6] on a log-log scale; the laminar regime is considered in Figure 1(a) and the turbulent regime in Figure 1(b). The experimental results are compared to the following conventional correlations: $f\,\mathrm{Re} = 64$ for circular tubes and $f\,\mathrm{Re} = 57$ for square channels, both for laminar flow, and the Blasius correlation, $f\,\mathrm{Re}^{-0.182} = 0.14$, for turbulent flow.

The results from heat transfer measurements on micro- and mini-channels from [4,6-11] are compared to the predictions from conventional correlations in Figure 2; the laminar regime is considered in Figure 2(a), and the turbulent regime in Figure 2(b). The theoretical predictions in the laminar regime are from $Nu = 1.86(\mathrm{Re}\,\mathrm{Pr})^{0.33}(D/L)^{0.33}$ (with L = 50 mm and D = 0.24 mm to obtain representative values), while the Dittus-Boelter correlation is used for predictions in the turbulent regime.

It is clear from Figures 1 and 2 that there is little agreement between the results from different investigators for either fluid flow or heat transfer in both laminar and turbulent regimes. Most of the experimental results deviate from the theoretical predictions which assume macroscale behavior. The measurements lie both above and below the predictions, and also show different trends of variation relative to the conventional predictions in the laminar and turbulent regimes. In addition, transition from the laminar to turbulent regimes appears to occur at lower Reynolds numbers in many

of the experimental studies relative to expectations from conventional analysis. These results have been cited to support the existence of differences in the physics at macro- and micro- length scales.

In view of the wide disparity in the literature on pressure drop and heat transfer in microchannels, carefully designed experiments were performed to understand the reasons for these discrepancies, as described in the following.

Fluid Flow Experiments

An experimental facility was designed to conduct fluid flow and heat transfer experiments in microchannels with hydraulic diameter ranging from 250 to 1000 μm. The aim of the experiments was to carefully analyze flow and heat transfer behavior in microchannels, verify the Reynolds numbers for transition from laminar to turbulent flow, and to assess the validity of the conventional correlations in predicting these characteristics.

Two different approaches were used in the fluid flow experiments. In the first, short microchannels were used with pressure taps placed at the inlet and outlet sections, beyond the length of the microchannel, as shown by the dashed lines in Figure 3. In the second, longer channels were tested, with pressure taps machined along the length of the microchannel itself, remote from the effects of the entrance and exit regions, as shown in Figure 3. The pressure drop measurements obtained from the short channels would include pressure losses due to the sudden contraction at the inlet and the expansion at the outlet of the channels. On the other hand, pressure drops obtained from the long channels would not include any additional losses. The details of the experimental setup and the uncertainty analysis for these experiments are available in [12].

The experimental results are reported in terms of Reynolds number, and friction factor, defined as $\mathrm{Re} = \frac{\rho U D_h}{\mu}$ and $f = \frac{(\Delta P/L)\, D_h}{\rho U^2/2}$, and compared to predictions from the following correlations for fully developed laminar and turbulent flow in channels of rectangular cross-section [13,14]:

$$f\,\mathrm{Re} = 96\left(1 - \frac{1.3553}{\alpha} + \frac{1.9467}{\alpha^2} - \frac{1.7012}{\alpha^3} + \frac{0.9564}{\alpha^4} - \frac{0.2537}{\alpha^5}\right) \quad (1)$$

and $f = 0.316/\mathrm{Re}^{0.25}$ for Re < 20,000. For cases involving both developing and fully developed flow in a channel, the apparent friction factor was calculated as:

$$f_{app}\,\mathrm{Re} = \left[\left\{\frac{3.2}{(x^+)^{0.57}}\right\}^2 + (f\,\mathrm{Re})_{fd}^{\,2}\right]^{1/2} \quad (2)$$

in which entrance length x^+ is given by $x^+ = L/(D_h\,\mathrm{Re})$. These correlations yield pressure drops in channels, without accounting for entrance and exit losses. As such, it is appropriate to compare these values directly with the measurements from the long microchannels considered (Figure 4), where the pressure taps are located within the channel. For the short channels, entrance and exit pressure losses are calculated as explained in [12] and subtracted from the measured values; the experimental results shown in Figure 5 are based on the measured pressure drops for the short channels, corrected for losses.

Fluid Flow Results

The experimentally determined friction factors are plotted against Reynolds number and compared to the predictions from correlations in Figure 4 for long channels of hydraulic diameters 974 µm and 324 µm. The figure shows clearly that the experimental results match the predictions quite well. Similar behavior was observed for channels of intermediate hydraulic diameters (324 µm

< D_h < 974 μm) as well. Moreover, it may be noted that the experimental friction factors start to deviate from the laminar predictions at Re ≈ 2000, indicating the onset of transition. This again indicates that the hydrodynamic behavior of the microchannels is not different from that of conventional channels in terms of transition.

The results from experiments on the short microchannels are presented in Figure 5 for channels of hydraulic diameter 244 μm. As stated earlier, the pressure losses due to entrance and exit have been subtracted from the measured values [12]. The good agreement between the modified experimental results and the theoretical predictions validates the methodology for the calculation of entrance and exit losses.

Flow visualization experiments were performed to verify the Reynolds number range for the onset of transition. The behavior of a dye streak injected through one of the pressure taps was used to identify the flow regime. If the dye streak maintained its integrity and remained well defined, the flow was considered laminar; when the dye streak starts to diffuse and blur, transition is considered to have started, with the whole channel cross-section being filled with dye in turbulent flow.

One set of visualizations is shown in Figure 6. At low Reynolds numbers (Re = 588, 1078), there is no diffusion of the dye streak along the length of the microchannel, and the streaklines have sharp edges. At Re = 1802, the edge of the dye streak starts to blur, indicating the onset of transition. By Re = 2202, the dye is almost completely diffused. Transition to turbulence in this case may be considered to have occurred at a Reynolds number of approximately 1800. These visualizations agree with the observations from the measured pressure drops, which showed that the flow stays laminar up to Re ≈ 2000.

Heat Transfer Experiments

The heat transfer experiments were performed using a copper heat sink with microchannels of hydraulic diameter ranging from 318 to 902 μm. The experimental setup was similar to that used for the fluid flow experiments, with modifications to allow for temperature measurements as described in [15]. The results of these experiments are reported in terms of Nusselt number, $\mathrm{Nu} = hD_h/k_f$. The average heat transfer coefficient h, was determined as $h = q/A\left(T_{m,w} - T_{m,f}\right)$, where the heat transferred to the coolant is $q = \rho c_p Q\left(T_{m,f,o} - T_{m,f,i}\right)$, the surface area of channels contributing to heat transfer is $A = nL\left(2H_c + W_c\right)$ and $T_{m,w} = T_w - qt/\left(k_s L_d W_d\right)$. The Reynolds number is calculated as for the fluid flow experiments.

The experimental results are compared to predictions for simultaneously developing laminar flow (both thermal and velocity boundary layers developing), thermally developing laminar flow (velocity boundary layer fully developed), and turbulent flow. The predictions for thermally developing laminar flow are obtained from the numerical work of Wibulswas [16]. For a rectangular channel heated on three sides with a uniform heat flux, the Nusselt number is given by: $\mathrm{Nu}_{x,3} = \mathrm{Nu}_{x,4}\left(\mathrm{Nu}_{fd,3}/\mathrm{Nu}_{fd,4}\right)$ [17]. The values of Nusselt number for developing laminar flow in 4-sides-heated channels ($\mathrm{Nu}_{x,4}$) and for fully developed flow in 3-sides- ($\mathrm{Nu}_{fd,3}$) and 4-sides- ($\mathrm{Nu}_{fd,4}$) heated channels, obtained from [16], were tabulated by Phillips [17]. These tables, as well as further details of the heat transfer experiments, are available in [15].

Predictions for the Nusselt number in turbulent flow are obtained from the Gnielinski correlation [18], valid for $0.5 < \mathrm{Pr} < 2000$ and $3000 < \mathrm{Re} < 5 \times 10^6$:

$$Nu_{turb} = \frac{\left(f_{turb}/8\right)\left(\mathrm{Re}_D - 1000\right)\mathrm{Pr}}{1 + 12.7\left(f_{turb}/8\right)^{1/2}\left(\mathrm{Pr}^{2/3} - 1\right)} \qquad (3)$$

The friction factor *f* for smooth pipes in the above is calculated using the expression due to Petukhov [19]:

$$f = \left(0.79\ln\left(\mathrm{Re}_D\right) - 1.64\right)^{-2} \tag{4}$$

Heat Transfer Results

Results from the heat transfer experiments are compared to predicted values in Figures 7 (a) and (b). The predictions include those for simultaneously and thermally developing laminar flows and for turbulent flow.

At low Reynolds numbers, the experimental results match the predictions for thermally developing laminar flow in both plots. As the Reynolds number increases, the experimental results depart from laminar predictions consistent with transition to a turbulent flow regime. For channels with a hydraulic diameter of 318 μm, the departure from thermally developing laminar behavior starts at Re = 1200, while as the hydraulic diameter increases, the experimental measurements follow the predicted thermally developing behavior all the way to a Reynolds number of 1800 (D_h = 902 μm).

Predicted Nusselt numbers from the Gnielinski correlation for turbulent flow lie significantly below the experimental values (Figure 7a). This was also observed to be true for experiments with channels of hydraulic diameters of 387, 501 and 564 μm, which are not presented here. Adams et al. [11,20] investigated single-phase forced convection of water in circular microchannels with diameters of 0.76, 1.09 and 1.13 mm. Their experimental Nusselt numbers for the smallest two sizes were also significantly higher than those predicted by the Gnielinski correlation. Interestingly, their data for the 1.13 mm channel was well predicted by the Gnielinski correlation, which led to the suggestion that a hydraulic diameter of approximately 1.2 mm is a reasonable lower limit for the

applicability of standard turbulent single-phase Nusselt-type correlations to non-circular channels. While the results of the present study are consistent with this suggestion, further experimentation will be necessary to resolve this issue.

PUMPING IN MICROCHANNELS

The pumping requirements for microchannel heat sinks are very high, which is considered one of the main reasons for microchannel heat sinks not to have seen widespread commercial use to date.

The pumping requirements of microchannel heat sinks are analyzed in this section. A graphical method to assess the suitability of candidate pumps for a particular microchannel heat sink application is presented. The microchannel dimensions are also optimized so that for a given heat removal rate, the pumping requirements of a heat sink are minimized.

The two primary thermal considerations in the design of microchannel heat sinks relate to the limits on the maximum temperature and the maximum temperature gradient on the chip. These may be expressed as:

1) The maximum temperature at any point on the chip should be less than T_{max}, i.e., $T_d < T_{max}$.
2) The maximum temperature gradient on the chip is limited to $\left(\frac{dT}{dx}\right)_{max}$, *i.e.*, $\left(\frac{dT}{dx}\right)_d < \left(\frac{dT}{dx}\right)_{max}$.

These two thermal limits can be used to calculate the limiting flow rate and the pressure head for given values of heat removal rate and channel dimensions [21].

Assuming fully developed hydrodynamic and thermal boundary layers in the microchannel, constant heat flux, equal participation of all four walls of each microchannel in heat transfer, fixed wall thickness between adjacent microchannels, and negligible deterioration in heat transfer due to fin inefficiencies, the minimum flow rate and minimum pressure head required to meet the two

thermal conditions while achieving a given heat removal rate (q Watts from a chip of length L_d and width W_d) are calculated. The minimum flow rate and the minimum pressure head from the limit on maximum temperature gradient are given by Eqs. (5) and (6), respectively, while those from the limit on maximum spot temperature are given by Eqs. (7) and (8), respectively. Also, Eq. (9) gives the flow rate versus pressure drop characteristics of a microchannel heat sink of given dimensions.

$$Q > \frac{q}{\rho c_p L_d \left(dT/dx\right)_{\max}} \tag{5}$$

$$\Delta p > \left(\frac{q\mu}{8\rho c_p W_d \left(dT/dx\right)_{\max}} \right) \frac{\left(1+\alpha\right)^2}{\alpha^3} f \,\mathrm{Re} \frac{w_c + w_w}{{w_c}^4} \tag{6}$$

$$Q > \left(\frac{q}{\rho c_p} \right) \frac{1}{\left(T_{\max} - T_{f,i} - \frac{q\left(w_c + w_w\right)}{\mathrm{Nu} k L_d W_d} \frac{\alpha}{\left(1+\alpha\right)^2} \right)} \tag{7}$$

$$\Delta p > \left(\frac{q\mu L_d}{8\rho c_p W_d} \right) \frac{\frac{\left(1+\alpha\right)^2}{\alpha^3} f \,\mathrm{Re} \frac{w_c + w_w}{{w_c}^4}}{\left(T_{\max} - T_{f,i} - \frac{q\left(w_c + w_w\right)}{\mathrm{Nu} k L_d W_d} \frac{\alpha}{\left(1+\alpha\right)^2} \right)} \tag{8}$$

$$\frac{\Delta p}{Q} = \frac{\mu L_d}{8 W_d} \frac{\left(1+\alpha\right)^2}{\alpha^3} f \,\mathrm{Re} \left(\frac{w_c + w_w}{{w_c}^4} \right) \tag{9}$$

A typical plot of pressure drop (Δp) versus total volume flow rate (Q) from these limits is shown in Figure 8 (a). The curves are plotted by varying the channel width for a given channel aspect ratio. The operating region of the microchannel heat sink is marked in Figure 8 (a). If the operating point of the microchannel heat sink, *i.e.*, the flow rate and pressure drop at which the microchannel heat sink operates, lies within the operating region, the desired heat transfer rate will be achieved and the limits on the maximum chip temperature and maximum temperature gradient will be met; otherwise,

one or more of these three conditions would not be satisfied. The boundary of the operating region labeled the minimum operating limit is shown in the figure.

The suitability of a pump to a microchannel heat sink design can be assessed by superimposing the pump curve and required flow rate versus pressure drop characteristics for the heat sink on a plot of the pumping requirements for the heat sink, as illustrated schematically in Figure 8 (b). The flow rate versus pressure drop characteristics of the microchannel heat sink are obtained from Eq. (5). The slope of these characteristics is a function of the microchannel dimensions. The point of intersection of these characteristics with the pump curve would be the operating point of the pump and heat sink. Only if the operating point lies in the operating region can the pump meet the desired conditions for the microchannel heat sink. Hence, for the example in Figure 8 (b), pump 1 in conjunction with microchannel heat sink 2 and 3 or pump 2 with microchannel heat sink 3 can dissipate the given heat load while satisfying the specified thermal constraints (points marked with open circles). The other pump-heat sink combinations would not work (points marked with solid circles). This approach provides a very simple way of assessing the suitability of any pump and microchannel heat sink for a desired application.

The point of intersection of the two limiting curves also represents the minimum pumping requirements of the microchannel heat sink, while satisfying the given thermal constraints. The microchannel width corresponding to this point, w_c^*, would be optimal for a prescribed aspect ratio, and the heat sink with these dimensions would impose the minimum requirements on the pump used to drive the fluid through the microchannels. This optimal width can be calculated by equating the flow rates from Eqs. (5) and (7) and is given by:

$$w_c^* = \frac{\mathrm{Nu} k L_d W_d}{q}\left(T_{\max} - T_{f,i} - L_d\left(\frac{dT}{dx}\right)_{\max}\right)\frac{(1+\alpha)^2}{\alpha} - w_w \qquad (10)$$

Review of Micropumping Techniques

One of the primary considerations in the implementation of microchannel heat sinks in practical applications is a need to understand and evaluate the competing methods for actuating the flow at the microscale. Integration of the pumping action directly at the scale of the microchannels in a heat sink is a very attractive alternative to the use of external pumps for driving the flow. A comprehensive review of the micropumping techniques available in the literature, with an emphasis on small-scale cooling applications, was generated by Singhal et al. [22]. The micropumps are compared qualitatively based on their working principles, limitations and advantages, and quantitatively in terms of the maximum achievable flow rate per unit cross-sectional area of the pump and the maximum achievable back pressure. The micropumps are also compared based on criteria such as miniaturization potential, size, actuation voltage and power required per unit flow rate, ease and cost of fabrication, minimum and maximum frequency of operation, and suitability to electronics cooling.

Some of the micropumps reviewed in [22] are compared based on their maximum flow rate per unit cross-sectional area (flow rate at zero back pressure) and maximum back pressure (back pressure at zero flow rate) in Figures 9 (a) and (b) [23-47]. Since compactness is the major concern in electronics cooling applications, the flow rate *per unit cross-sectional area of the pump* is plotted. Only the cross-sectional area of the pumping chamber is considered for vibrating diaphragm micropumps [23-36], and the cross-sectional area of the electrodes or that of the channel under the electric/magnetic field is used for the EHD [37-39], MHD [40] and electroosmotic pumps [41,42].

Figure 9 (a) shows that the pumps with the highest flow rate per unit area are the injection-type EHD, electroosmotic, flexural plate wave, piezoelectric, rotary and valveless micropumps.

However, the high flow rates obtained in some of the pumps using surface effects such as electroosmotic [41] and flexural plate wave [45] can be attributed to their use of shallow channels. These pump designs would require very large surface areas to achieve required flow rates, and potentially render them infeasible in most electronics cooling applications. From Figure 9 (b), it can be seen that piezoelectric, electroosmotic and valveless micropumps yield the highest back pressures. From this simplified viewpoint of maximum flow rate and pressure head, valveless, piezoelectric and electroosmotic micropumps appear to be the most suitable for electronics cooling. More details of the comparison of micropumps in the literature are available in [22].

ONGOING AND FUTURE WORK

A novel Infra-Red Micro Particle Image Velocimetry (IR-μPIV) technique is being developed for investigating local velocity and temperature fields in microchannels. μPIV is a non-invasive measurement technique and is particularly suited to MEMS and microfluidic devices. However, its application with visible light requires optical access to the flow. Since silicon is essentially transparent to infra-red light, the IR-μPIV technique allows measurements within silicon-based micro-devices [48], which are opaque to visible light. Detailed local velocity measurements are being obtained inside microchannels, which will provide an improved understanding of the transport processes. One of the objectives of this work is to extend the technique to the measurement of significantly higher velocities than have been investigated to date. Furthermore, Brownian motion of tracer particles used in the PIV experiments is a function of the local temperature of the fluid. The "noise" caused by Brownian motion causes changes in the cross-correlation peaks in the PIV results, which can be detected [49] and potentially interpreted to obtain local temperature fields inside the silicon structures.

A new integrated microchannel heat sink concept, in which micropumps are integrated into the cooling channels, is also being developed. In addition, several novel micropump designs especially suited for high-heat-flux electronics cooling applications are under development in the authors' group.

Acknowledgements

The authors acknowledge the financial support from members of the Cooling Technologies Research Center (http://widget.ecn.purdue.edu/~CTRC), a National Science Foundation Industry/University Cooperative Research Center at Purdue University for a large part of this work. Assistance from Dong Liu and Poh-Seng Lee on the sections on fluid flow and heat transfer is also acknowledged.

REFERENCES

[1] Garimella, S. V., and Sobhan, C. B., Transport in microchannels – A critical review, *Annual Review of Heat Transfer*, vol. 13, 2003.

[2] Sobhan, C. B., and Garimella, S. V., A comparative analysis of studies on heat transfer and fluid flow in microchannels, *Microscale Thermophysical Engineering*, vol. 5, pp. 293-311, 2001.

[3] Wu, P. Y., and Little, W. A., Measurement of friction factor for the flow of gases in very fine channels used for micro miniature Joule Thompson refrigerators, *Cryogenics*, vol. 23, pp. 273-277, 1983.

[4] Choi, S. B., Barron, R. F., and Warrington, R. O., Fluid flow and heat transfer in microtubes, *Micromechanical Sensors, Actuators and Systems,* ASME DSC-vol.32, pp. 123-134, 1991.

[5] Peng, X. F., Peterson, G. P., and Wang, B. X., Frictional flow characteristics of water flowing through microchannels, *Experimental Heat Transfer,* vol. 7, pp. 249-264, 1994.

[6] Yu, D., Warrington, R., Barron, R., and Ameel, T., An experimental and theoretical investigation of fluid flow and heat transfer in microtubes, *ASME/JSME Thermal Engineering Conference*, vol. 1, pp. 523-530, 1995.

[7] Wu, P. Y., and Little, W. A., Measurement of the heat transfer characteristics of gas flow in fine channel heat exchangers for micro miniature refrigerators, *Cryogenics*, vol. 24, pp. 415-420, 1984.

[8] Wang, B. X., and Peng, X. F., Experimental investigation on liquid forced convection heat transfer through microchannels, *International Journal of Heat and Mass Transfer,* vol. 37, Suppl. 1, pp.73-82, 1994.

[9] Peng, X. F., Peterson, G. P., and Wang, B. X., Heat transfer characteristics of water flowing through microchannels, *Experimental Heat Transfer,* vol. 7, pp. 265-283, 1994.

[10] Peng, X. F., and Peterson, G. P., Convective heat transfer and flow friction for water flow in microchannel structures, *International Journal of Heat and Mass Transfer,* vol. 39, pp. 2599-2608, 1996.

[11] Adams, T. M., Abdel-Khalik, S. I., Jeter, S. M., and Qureshi, Z. H., An experimental investigation of single-phase forced convection in microchannels, *International Journal of Heat and Mass Transfer,* vol. 41, pp. 851-857, 1998.

[12] Liu, D., and Garimella, S. V., Investigation of liquid flow in microchannels, *8th AIAA/ASME Joint Thermophysics and Heat Transfer Conference*, St. Louis, Missouri, Paper No. AIAA 2002-2776, pp. 1-10, 2002.

[13] Shah, R. K., and London, A. L., Laminar flow forced convection in ducts, *Advances in Heat Transfer*, Supplement 1, Academic Press, 1978.

[14] Incropera, F. P., and DeWitt, D. P., *Fundamentals of Heat and Mass Transfer*, 4th ed., John Wiley & Sons, New York, 1998.

[15] Lee, P.-S., and Garimella, S. V., Experimental investigation of heat transfer in microchannels, *ASME Summer Heat Transfer Conference, Las Vegas, Nevada,* 2003.

[16] Wibulswas, P., Laminar Flow Heat Transfer In Non-Circular Ducts, Ph.D. Thesis, University College, London, 1966.

[17] Phillips, R. J., Microchannel Heat Sinks, Ph.D. Thesis, Massachusetts Institute of Technology, Cambridge, MA, 1987.

[18] Gnielinski, V., New equations for heat and mass transfer in turbulent pipe and channel flow, *International Chemical Engineering*, vol. 16, pp. 359-368, 1976.

[19] Petukhov, B. S., Heat transfer and friction in turbulent pipe flow with variable physical properties, *Advances in Heat Transfer,* Vol. 6, pp. 503-565, 1970.

[20] Adams, T. M., Dowling, M. F., Abdel-Khalik, S. I., and Jeter, S. M., Applicability of traditional turbulent single phase forced convection correlations to non-circular microchannels, *International Journal of Heat and Mass Transfer*, vol. 42, pp. 4411-4415, 1999.

[21] Singhal, V., Liu, D., and Garimella, S. V., Analysis of pumping requirements for microchannel cooling systems, *Proceedings of International Electronic Packaging Technical Conference and Exhibition (InterPACK)*, Maui, Hawaii, 2003.

[22] Singhal, V., Garimella, S. V., and Raman, A., Microscale pumping technologies for microchannel cooling systems, *Applied Mechanics Reviews*, 2003, (in review).

[23] Esashi, M., Shoji, S., and Nakano, A., Normally closed microvalve and mircopump fabricated on a silicon wafer, *Sensors and Actuators*, vol. 20, pp. 163-169, 1989.

[24] Zengerle, R., Ulrich, J., Kluge, S., Richter, M., and Richter, A., A bidirectional silicon micropump, *Sensors and Actuators A: Physical*, vol. 50, pp. 81-86, 1995.

[25] Stehr, M., Messner, S., Sandmaier, H., and Zengerle, R., The VAMP - A new device for handling liquids or gases, *Sensors and Actuators A: Physical*, Vol. 57, pp. 153-157, 1996.

[26] Olsson, A., Enoksson, P., Stemme, G., Stemme, E., Micromachined flat-walled valveless diffuser pumps, *Journal of Microelectromechanical Systems*, vol. 6, pp. 161-166, 1997.

[27] Bardell, R. L., Sharma, N. R., Forster, F. K., Afromowitz, M. A., and Penney R. J., Designing high-performance micro-pumps based on no-moving-parts valves, *Microelectromechanical Systems, ASME DSC 62/HTD 354*, pp.47-53, 1997.

[28] Dewa, A. S., Deng, K., Ritter, D. C., Bonham, C., Guckel, H., and Massood-Ansari, S., Development of LIGA-fabricated, self-priming, in-line gear pumps, *Transducers'97, Chicago*, pp. 757-760, 1997.

[29] Kaemper, K.-P., Doepper, J., Ehrfeld, W., and Oberbeck, S., Self-filling low-cost membrane micropump, *Proceedings of the IEEE Micro Electro Mechanical Systems*, pp. 432-437, 1998.

[30] Koch, M., Harris, N., Evans, A. G. R., White, N. M., and Brunnschweiler, A., A novel micromachined pump based on thick-film piezoelectric actuation, *Sensors and Actuators A: Physical*, vol. 70, pp. 98-103, 1998.

[31] Böhm, S., Olthuis, W., and Bergveld, P., A plastic micropump constructed with conventional techniques and materials, *Sensors and Actuators A: Physical*, vol. 77, pp. 223-228, 1999.

[32] Li, H. Q., Roberts, D. C., Steyn, J. L., Turner K. T., Carretero, J. A., Yaglioglu, O., Su, Y. H., Saggere, L., Haggod, N. W., Spearing, S. M., Schmidt, M. A., Mlcak, R., and Breuer, K. S., A high frequency high flow rate piezoelectrically driven MEMS micropump, *Solid-State Sensor & Actuator Workshop, Hilton Head, South Carolina*, pp. 69-72, 2000.

[33] Schabmueller, C. G. J., Koch, M., Evans, A. G. R., Brunnschweiler, A., and Kraft, M., Design and fabrication of a self-aligning gas/liquid micropump, *Proceedings of SPIE - The International Society for Optical Engineering*, Vol. 4177, pp. 282-290, 2000.

[34] Xu, D., Wang, L., Ding, G., Zhou, Y., Yu A., and Cai, B., Characteristics and fabrication of NiTi/Si diaphragm micropump, *Sensors and Actuators A: Physical*, vol. 93, pp. 87-92, 2001.

[35] Wego, A., and Pagel, L., A self-filling micropump based on PCB technology, *Sensors and Actuators A: Physical*, Vol. 88, pp. 220-226, 2001.

[36] Yun, K.-S., Cho, I.-J., Bu, J.-U., Kim, G.-H., Jeon, Y.-S., Kim, C.-J., and Yoon, E., A micropump driven by continuous electrowetting actuation for low voltage and low power operations, *Proceedings of the IEEE Micro Electro Mechanical Systems (MEMS)*, pp. 487-490, 2001.

[37] Richter, A., Plettner, A., Hofmann, K. A., and Sandmaier, H., A micromachined electrohydrodynamic (EHD) pump, *Sensors and Actuators A: Physical*, Vol. 29, pp. 159-168, 1991.

[38] Fuhr G., Hagedorn, R., Mullerm, T., Benecke, W., and Wagner, B., Microfabricated electrohydrodynamic (EHD) pumps for liquids of higher conductivity, *Journal of Microelectromechanical Systems*, vol. 1, 141-146, 1992.

[39] Darabi, J., Ohadi, M. M., and DeVoe, D., An electrohydrodynamic polarization micropump for electronic cooling, *Journal of Microelectromechanical Systems*, vol. 10, pp. 98-106, 2001.

[40] Lemoff, A. V., and Lee, A. P., An AC magnetohydrodynamic micropump, *Sensors and Actuators B: Chemical*, Vol. 63, pp. 178-185, 2000.

[41] Chen, C. H., Zeng, S., Mikkelsen, J. C., and Santiago, J. G., Development of a planar electrokinetic micropump, *Proceedings of ASME International Mechanical Engineering Congress and Exposition, Orlando, Florida*, MEMS **1**, pp. 523-528, 2000.

[42] Zeng, S., Chen, C.-H., Santiago, J. G., Chen, J.-R., Zare, R. N., Tripp, J. A., Svec, F., and Fréchet, J. M. J., Electroosmotic flow pumps with polymer frits, *Sensors and Actuators B: Chemical*, Vol. 82, pp. 209-212, 2002.

[43] Ahn, C. H., and Allen M. G., Fluid micropumps based on rotary magnetic actuators, *Proceedings of the IEEE Micro Electro Mechanical Systems (MEMS), Amsterdam, the Netherlands*, pp. 408-412, 1995.

[44] Grosjean, C., and Tai, Y.-C., A thermopneumatic peristaltic micropump, *Transducers' 99, Sendai, Japan*, pp. 1776-1779, 1999.

[45] Black, J. P., and White, R. M., Microfluidic applications of ultrasonic flexural plate waves, *Transducers' 99 Conference, Sendai, Japan*, pp. 1134-1136, 1999.

[46] Geng, X., Yuan, H., Oguz, H. N., and Prosperetti, A., Bubble-based micropump for electrically conducting liquids, *Journal of Micromechanics and Microengineering*, vol. 11, pp. 270-276, 2001.

[47] Tsai, J.-H., and Lin, L., A thermal bubble actuated micro nozzle-diffuser pump, *Proceedings of the IEEE Micro Electro Mechanical Systems (MEMS), Interlaken, Switzerland*, pp. 409-412, 2001.

[48] Han, G., Bird, J. C., Johan, K., Westin, A., and Breuer, K. S., Infrared diagnostics for measuring fluid and solid motion inside MEMS, *Proceedings of the IEEE Workshop on Solid State Sensors and Actuators, Hilton Head, SC,* 2002.

[49] Gui, L., Wereley, S. T., and Lee, S. Y., Simultaneous, spatially-resolved temperature and velocity measurements using cross-correlation PIV, *Proceedings of the 11th International Symposium on the Application of Laser Techniques to Fluid Mechanics, Lisbon, Portugal,* Paper 15.1, 2002.

LIST OF FIGURES

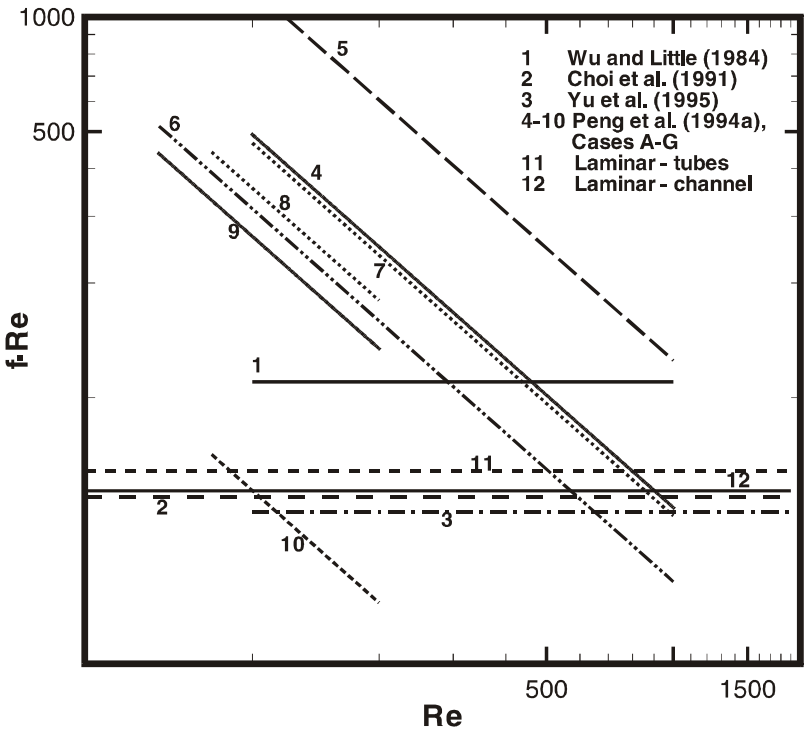

(a)

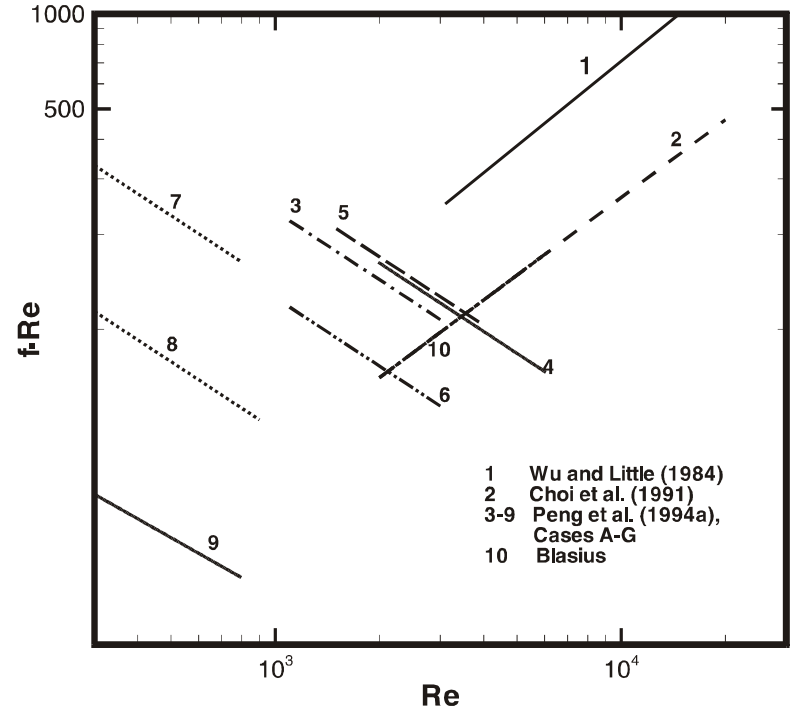

(b)

Figure 1. Comparison of friction factor from experimental results and theoretical predictions for (a) laminar; and (b) turbulent flow in microchannels and microtubes [2].

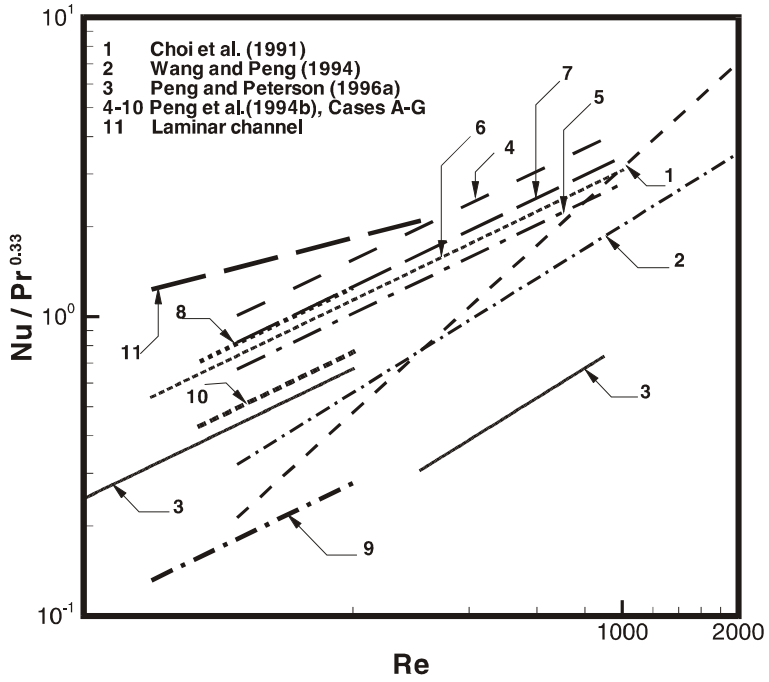

(a)

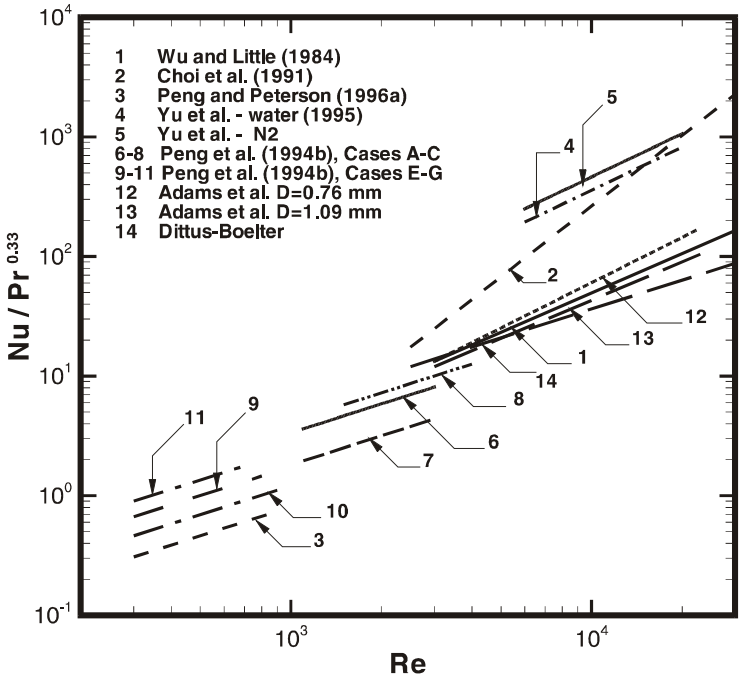

(b)

Figure 2. Comparison of heat transfer from experimental results and theoretical predictions for (a) laminar; and (b) turbulent flow in microchannels and microtubes [2].

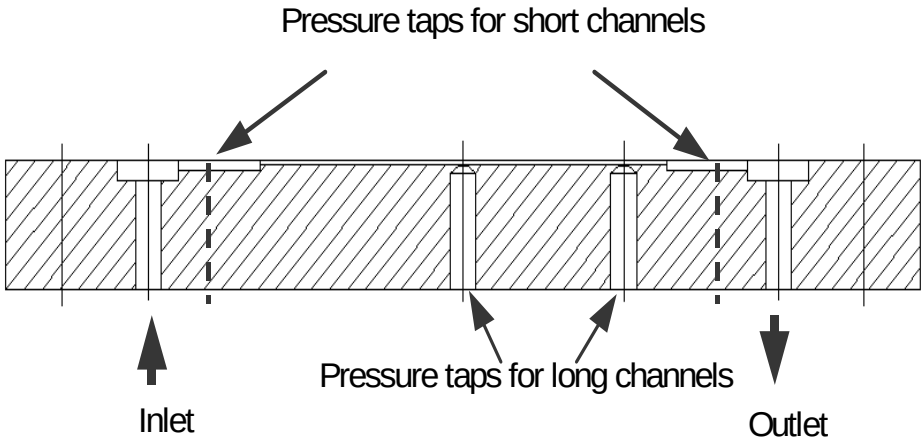

Figure 3. A schematic of the microchannel test section of second type.

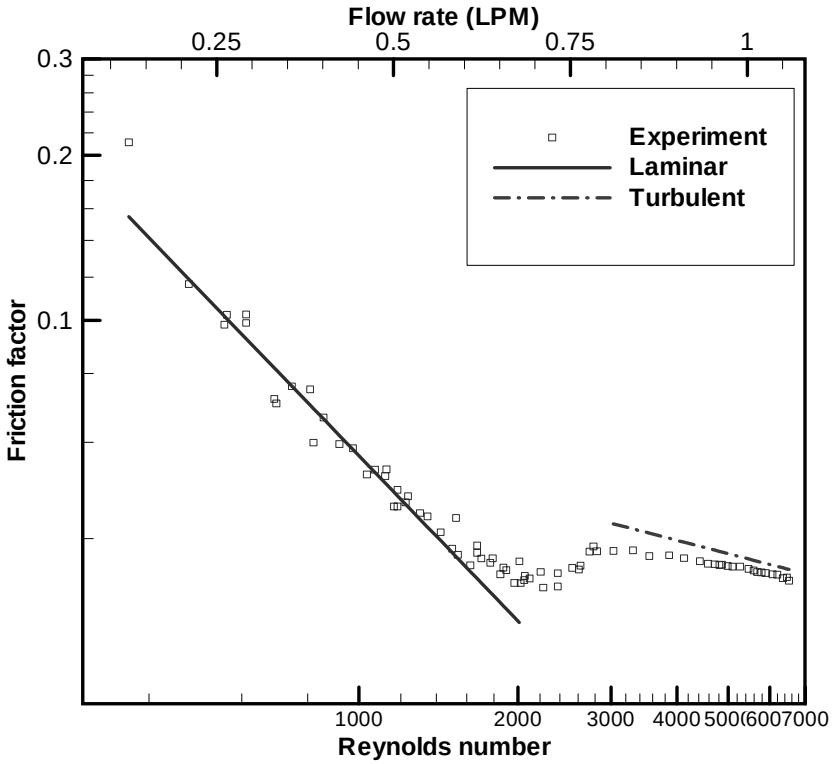

(a)

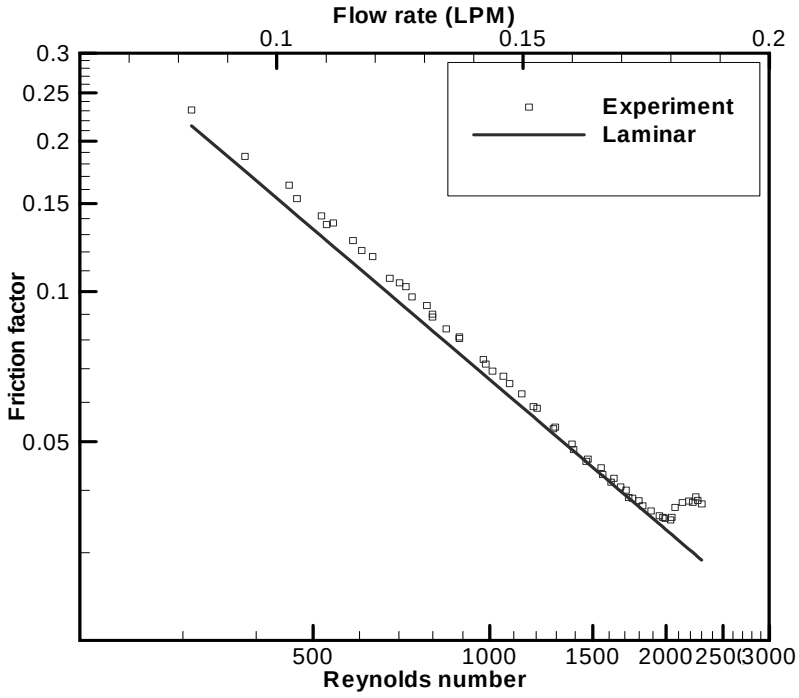

(b)

Figure 4. Variation of friction factor with Reynolds number for long microchannels: comparison of experiments with and theory for D_h of (a) 974 µm, and (b) 324 µm [12].

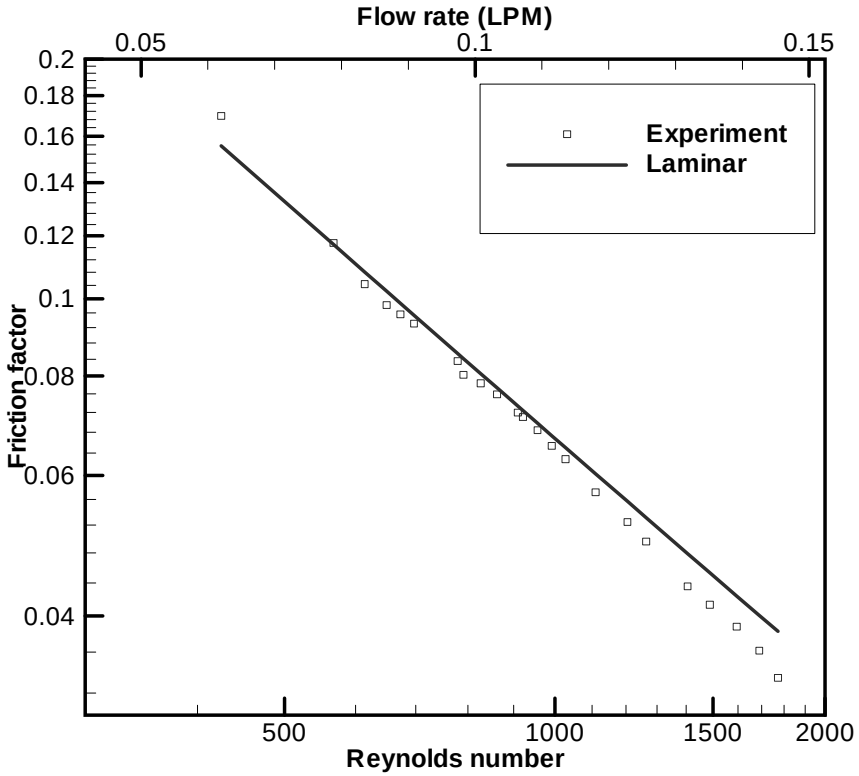

Figure 5. Variation of friction factor with Reynolds number: comparison of experiments and theory for short channels of D_h = 244 μm [12].

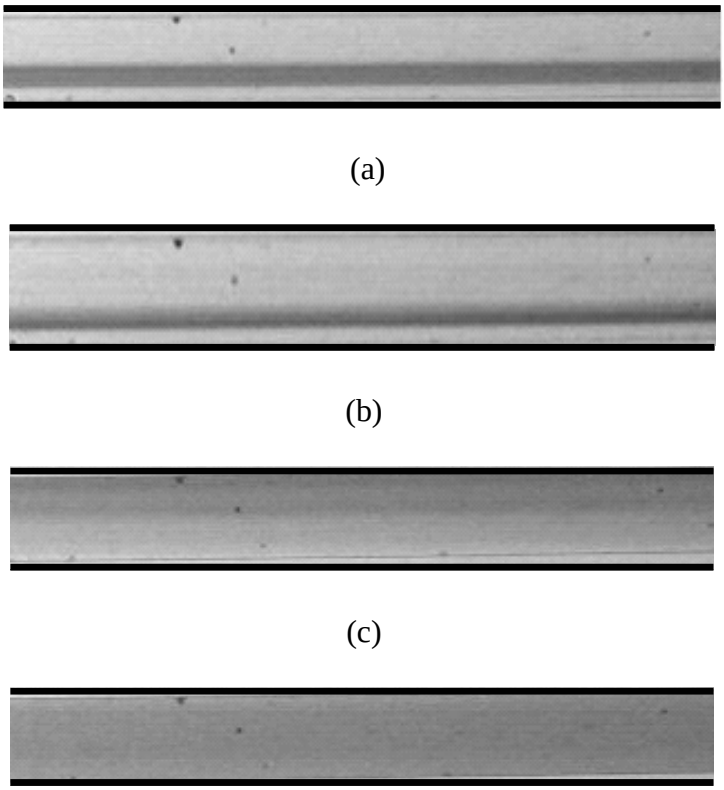

Figure 6. Flow visualization results in a microchannel with D_h = 470 μm [12]: (a) Re = 588 (78 ml/min) laminar flow, (b) Re = 1078 (143 ml/min) laminar flow, (c) Re = 1802 (239 ml/min) transitional flow and (d) Re = 2202 (292 ml/min) turbulent flow.

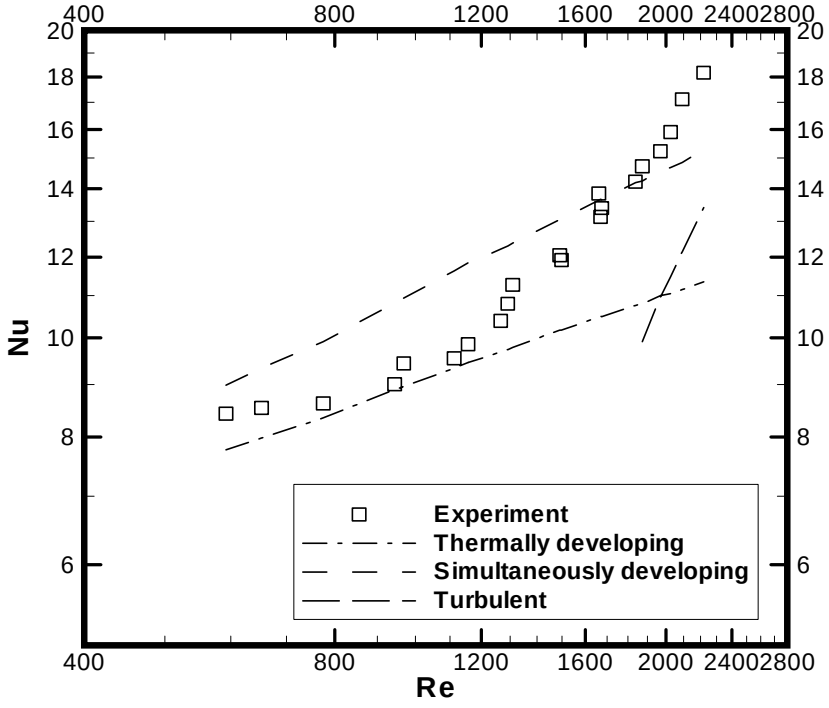

(a)

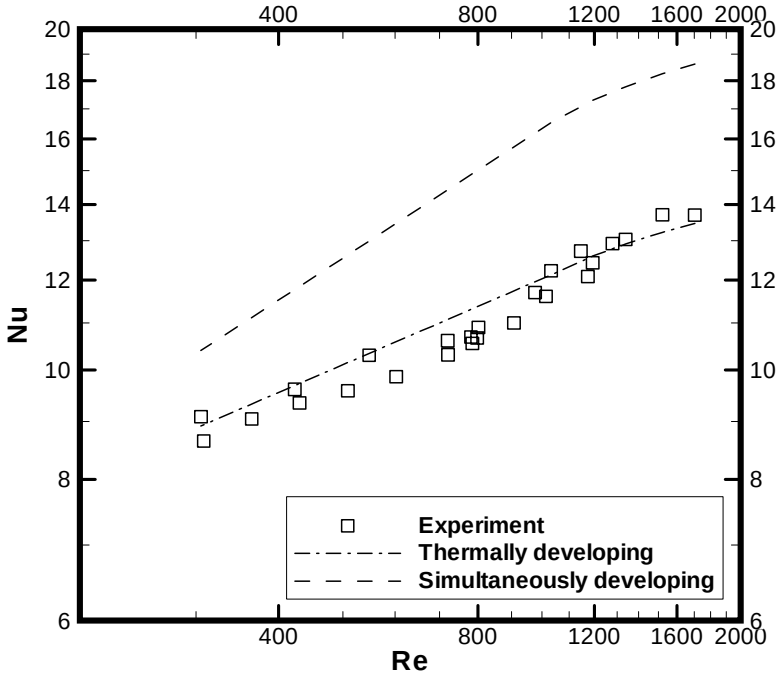

(b)

Figure 7. Variation of Nusselt number with Reynolds number: Comparison of experiments with theory for channels of (a) D_h = 318 µm (W_c = 194 µm), and (b) D_h = 902 µm (W_c = 534 µm) [15].

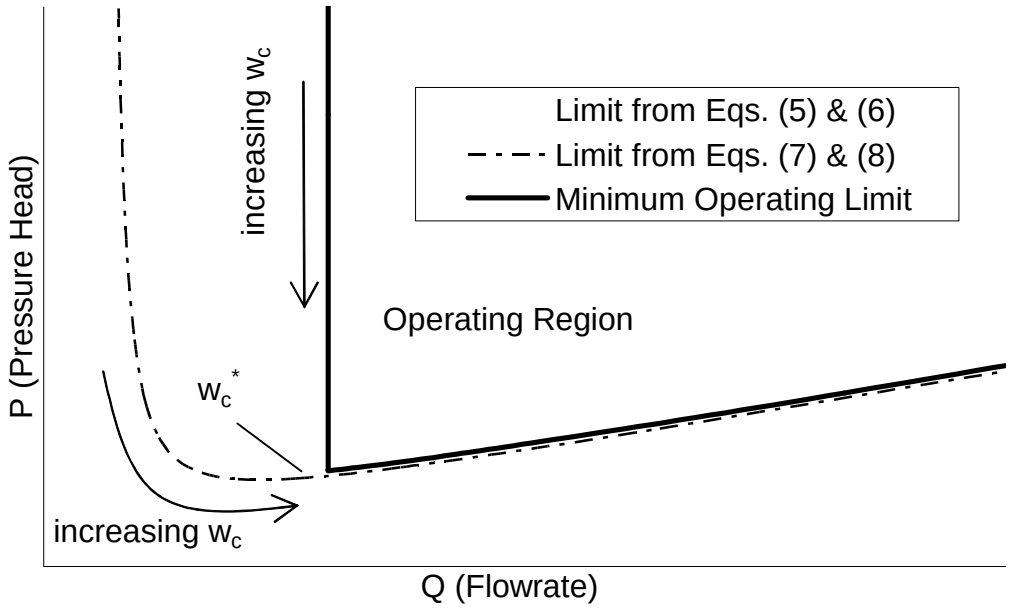

(a)

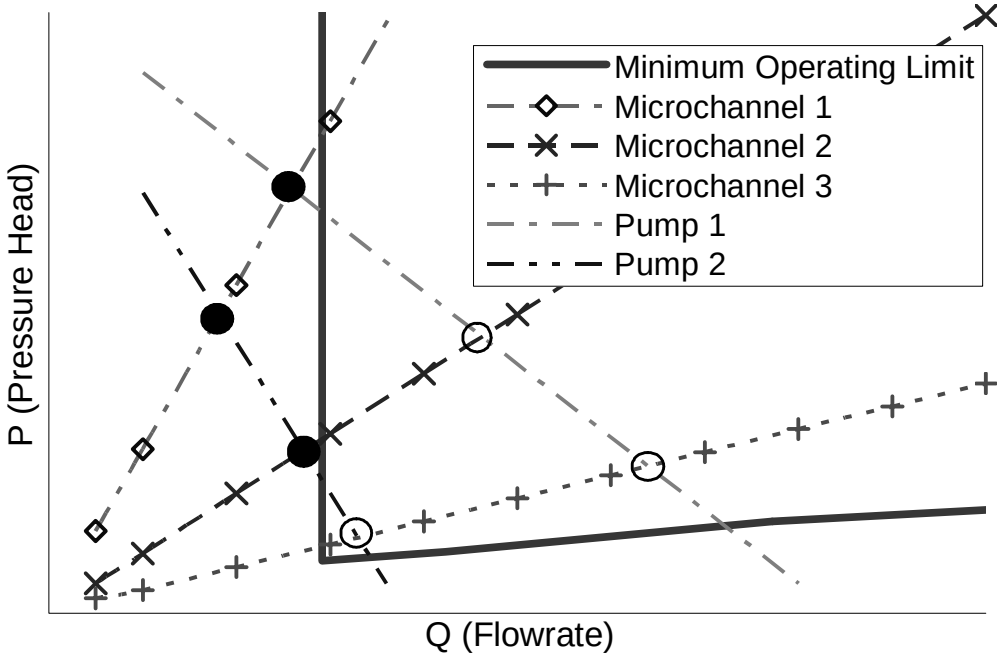

(b)

Figure 8. (a) Pumping requirements of microchannel heat sinks of fixed aspect ratio; and (b) Plot for checking the suitability of pumps to microchannel heat sinks of fixed aspect ratio [21].

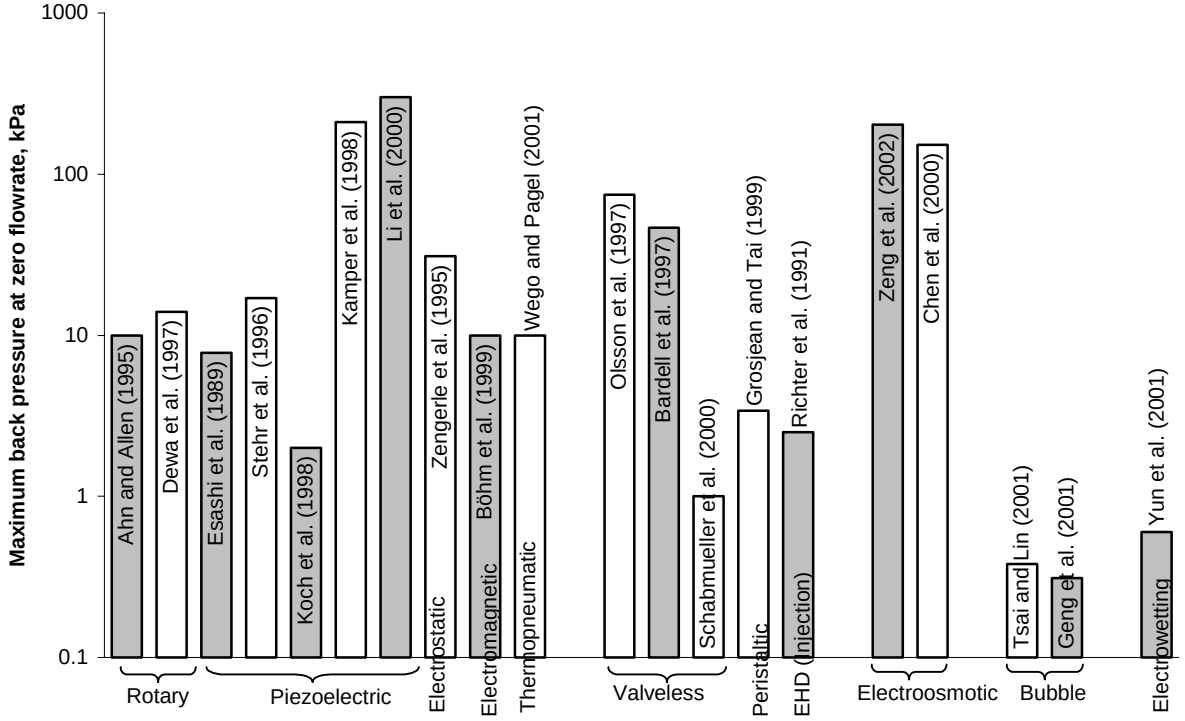

(a)

Figure 9. (a) Maximum flow rate per unit cross-sectional area at zero back pressure, and (b) maximum back pressure at zero flow rate of various micropumps presented in literature. The maximum back pressure was not reported for the Shape Memory Alloy pump [34], Induction-type EHD pump [38], MHD pump [40] and Flexural Plate Wave pump [45].

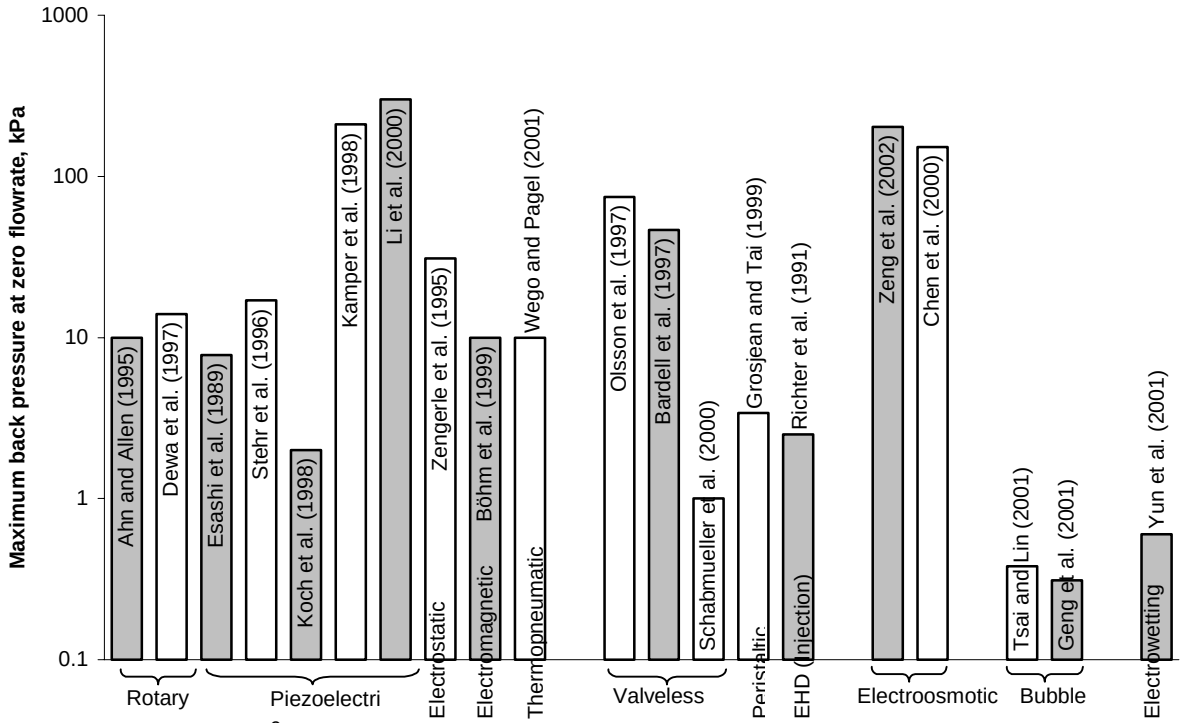

(b)

Figure 9 (cont'd). (a) Maximum flow rate per unit cross-sectional area at zero back pressure, and (b) maximum back pressure at zero flow rate of various micropumps presented in literature. The maximum back pressure was not reported for the Shape Memory Alloy pump [34], Induction-type EHD pump [38], MHD pump [40] and Flexural Plate Wave pump [45].